MED13L pathogenic missense variants impair protein stability and interaction, underlying diverse clinical outcomes

Thomas Smol, Frédéric Frenois, Morgane Billotte, Roseline Caumes, Leonie Menke, Amara Nassar-Sheikh Rashid, Caroline Thuillier, Didier Monté, Florence Petit, Alexis Verger, et al.

HGG Advances

ARTICLE

MED13L pathogenic missense variants impair protein stability and interaction, underlying diverse clinical outcomes

Thomas Smol,[1,4,*] Frédéric Frenois,[1] Morgane Billotte,[1] Roseline Caumes,[1] Leonie A. Menke,[2] Amara Nassar-Sheikh Rashid,[2] Caroline Thuillier,[1] Didier Monté,[3] Florence Petit,[1] Alexis Verger,[3] and Jamal Ghoumid[1,*]

Summary

Heterozygous pathogenic variants in the Mediator complex subunit 13-like gene located in the *locus* 12q21.21 (*MED13L*) are associated with intellectual disability, developmental delay, and distinctive facial features. While nonsense and frameshift variants typically cause haploinsufficiency, resulting in a well-characterized clinical presentation, missense variants have been associated with a broader range of phenotypes, including epilepsy and severe motor delay. In this study, we investigated five pathogenic missense variants in *MED13L*—c.2597C>T p.Pro866Leu, c.2605C>T p.Pro869Ser, c.3392G>A p.Cys1131Tyr, c.5695G>A p.Gly1899Arg, and c.6485C>T p.Thr2162Met—associated with different clinical severities. We identified significant reductions in protein stability across these variants, with some exhibiting aberrant cytoplasmic localization, suggesting disruptions in structural integrity and function. In particular, exon 15 variants (p.Pro866Leu and p.Pro869Ser) correlated with severe phenotypes, including epilepsy and severe motor impairment, whereas p.Gly1899Arg and p.Thr2162Met were associated with milder manifestations. 3D protein modeling suggested that these missense variants may disrupt MED13L's interaction with the CDK8 kinase module, leading to functional deficits. Our findings highlight different pathogenic mechanisms, ranging from protein instability to altered molecular interactions, that contribute to the clinical variability observed in MED13L-related disorders.

Introduction

Heterozygous pathogenic variants of the Mediator complex subunit 13-like gene located in the *locus* 12q21.21 (*MED13L*; MIM: 608771), which result in haploinsufficiency, have been identified as the cause of MED13L-related intellectual disability in patients presenting with moderate to severe global developmental delay, distinctive facial features, and, in some cases, cardiac defects (MIM: 616789).[1–7] Heterozygous nonsense or frameshift variants leading to a loss of function have been associated with the condition.[1,2,4] Then, several pathogenic missense variants clustered in exons 15–17, 25, and 27–31 have been reported in patients with a broader clinical phenotype, including epilepsy and severe gross motor delay.[5–7]

The functions of the MED13L protein remain partially unresolved, and the precise functional consequences of missense pathogenic variants remain unknown. The encoded protein is a paralog of MED13 (MIM: 603808), another subunit of the Mediator complex.[2,8] Both subunits are components of the highly conserved CDK8 kinase module (CKM), along with MED12 (MIM: 300188) or its paralog MED12L (MIM: 611318), CDK8 (MIM: 603184) or its paralog CDK19 (MIM: 614720), and cyclin-C (MIM: 123838).[9] The CKM is thought to be involved in repressing gene expression by preventing interactions between the core Mediator complex and RNA polymerase II (RNA Pol II).[10] MED13 and MED13L mediate the integration of the CKM into the core Mediator complex, in particular by interacting with MED19 (MIM: 612385) and regulating the interaction between MED26 (MIM: 605043) and the carboxyl-terminal domain of RNA polymerase through their intrinsically disordered regions (IDRs).[10–12] Within the CKM, MED13L can replace MED13 and, conversely, can do so in an exclusive manner depending on the cellular context.[13] Dissociation of the CKM from the core Mediator complex is mediated by MED13 or MED13L degradation through a ubiquitin-proteasome-mediated mechanism.[9] Subsequently, association of the core Mediator complex with RNA Pol II can be achieved for gene transcription.[11,14]

We aimed to elucidate the mechanisms associated with the pathogenic *MED13L* missense variants. We selected five variants located in exons 15, 17, and 30 that cause either a severe or a typical *MED13L* syndrome phenotype: c.2597C>T p.Pro866Leu,[6] c.2605C>A p.Pro869Ser,[6,8] c.3392G>A p.Cys1131Tyr,[7] c.5695G>A p.Gly1899Arg,[15,16] and c.6485C>T p.Thr2162Met.[16,17]

[1]University Lille, CHU Lille, ULR7364 – RADEME – Maladies Rares du Développement Embryonnaire, 59000 Lille, France; [2]Amsterdam UMC, location University of Amsterdam, Emma Children's Hospital, Department of Pediatrics, Emma Center for Personalized Medicine, Amsterdam Neuroscience - Cellular & Molecular Mechanism, Amsterdam Reproduction & Development, Meibergdreef 9, Amsterdam, the Netherlands; [3]CNRS EMR 9002 Integrative Structural Biology, INSERM U1167 – RID-AGE, University Lille, CHU Lille, Institut Pasteur de Lille, 59000 Lille, France
[4]Lead contact
*Correspondence: thomas.smol@univ-lille.fr (T.S.), jamal.ghoumid@univ-lille.fr (J.G.)
https://doi.org/10.1016/j.xhgg.2025.100467.

We observed that different mechanisms may be involved in the pathogenicity of missense variants, leading to a loss of function correlating with disease severity.

Methods

Patient and molecular data

Patient clinical and genetic data used for these studies were previously reported in other publications or databases. The five missense variants analyzed in this study—p.Pro866Leu, p.Pro869Ser, p.Cys1131Tyr, p.Gly1899Arg, and p.Thr2162Met— have been previously described as pathogenic or likely pathogenic. They were selected based on their clinical recurrence in public databases (ClinVar and HGMD), phenotypic relevance, and functional domain representation.[6–8,15–25] Variants such as p.Pro866Leu, p.Gly1899Arg, and p.Thr2162Met have been reported in multiple individuals, while p.Pro869 is a mutational hotspot with multiple pathogenic substitutions. Although p.Cys1131Tyr is not recurrent, it was included due to its association with a notably severe phenotype, allowing us to explore potential variant-specific effects.[7] Among the patients included in this study, one individual carrying the recurrent c.2606C>T p.Pro869Leu variant represents a previously unpublished case (P6, supplemental note). Written informed consent for the publication of clinical and genetic data was obtained from the patient's parents in accordance with institutional ethical guidelines.

Plasmid construction

An expression plasmid containing the full-length 6,633 bp cDNA for the human *MED13L* gene (GenBank: NM_015335.5) with an N-terminal triple 3xFLAG tag was custom designed and obtained from VectorBuilder (Cyagen Biosciences, Santa Clara, CA, USA) for transfection assays. The Q5 Site-Directed Mutagenesis Kit from NEB (New England Biolabs, Ipswich, MA, USA) was used to introduce single-nucleotide variants into the wild—type (WT) *MED13L* plasmid expression vector sequence according to the manufacturer's protocol. Mutagenic primers were designed using the NEBaseChanger tool available online to analyze the previously described pathogenic missense variants p.Pro866Leu,[6] p.Pro869Ser,[6,8] p.Cys1131Tyr,[7] p.Gly1899Arg,[15,16] and p.Thr2162Met.[16,17] All mutagenesis products were confirmed by Sanger sequencing.

Cell culture and transfection

HEK293 cell lines were cultured in DMEM supplemented with 10% fetal bovine serum, 2 mM L—glutamine, 100 UI/mL penicillin, and 100 μg/mL streptomycin at 37°C with 5% CO_2. Plasmids were transfected using Lipofectamine 2000 (Thermo Fisher Scientific, Waltham, MA, USA) according to the manufacturer's instructions. The day before transfection, 0.5×10^6 cells were plated in 6-well plates. Cells were then transfected with 2 μg of plasmid DNA containing either WT sequences or mutant sequences. Experiments were performed in triplicate.

Western blot analysis

Cells were harvested 96 h after transfection. HEK293 cells were then lysed in ice-cold lysis RIPA (Radio-ImmunoPrecipitation Assay) buffer complemented with Complete Protease Inhibitor Cocktail (Roche Life Science, Penzberg, Germany). The lysates were centrifuged at 20,000 rpm for 10 min at 4°C. The supernatants were separated from the debris, and the protein concentration was determined by the BCA (BiCinchoninic Acid) method. For each condition, 20 μg of total proteins was mixed with NuPAGE LDS Sample Buffer 4× (Thermo Fisher Scientific) and heated at 100°C for 5 min. Denatured proteins were separated on NuPAGE 3%–8% tris-acetate protein gels (Thermo Fisher Scientific) and transferred to a nitrocellulose membrane. Blots were incubated overnight at 4°C with monoclonal anti-FLAG M2 antibody (1:500; Sigma-Aldrich, St. Louis, MO, USA) for 3xFLAG-MED13L detection and monoclonal β-tubulin antibody (1:5,000; CliniSciences, Nanterre, France) as a control. Membranes were then incubated with secondary antibody goat anti-mouse immunoglobulin (Ig)G (H+L) and HRP conjugated (SouthernBiotech, Birmingham, AL, USA) for 1 h at RT and revealed with SuperSignal West Dura Extended Duration Substrate (Thermo Fisher Scientific). Quantification was performed using the ImageJ software (Rasband, Bethesda, MD, USA). All experiments were performed in triplicate.

Co-immunoprecipitation

HEK293 human cells were transfected with 6 μg of pcDNA3 3xFLAG WT and mutant *MED13L* plasmids using Lipofectamine 3000 based on the manufacturer's recommendations. Mock-transfected cells were used as controls. After 24 h, cells were washed with phosphate-buffered saline (PBS) and lysed in 1 mL buffer containing 50 mM Tris/HCl (pH 8), 250 mM NaCl, 1 mM EDTA, 1 mM TCEP, 10% glycerol, 3 mM $MgCl_2$, and 0.1% Igepal CA-630. After centrifugation, the extracted proteins were incubated with 30 μL of anti—FLAG M2 affinity gel (Sigma A2220) on a rotating wheel overnight at 4°C. After extensive washing, the precipitated proteins were identified by western blot. The antibodies used to detect Mediator subunits were from Bethyl Laboratories (anti—Med12 A300—774A [1:5,000], anti-cyclin C A301—989A [1:5,000], and anti—CDK8 A302—500A [1:2,500]). The antibody used to detect FLAG hMED13L derivatives was from Sigma (monoclonal anti-FLAG M2 peroxidase [HPR] A8592 [1:10,000]). Western blot was performed using an ECL kit (Amersham GE Healthcare Life Sciences) according to the manufacturer's recommendations. HRP—conjugated secondary antibodies were used at 1:5,000 and were purchased from Amersham GE Healthcare Life Sciences. All the membranes were scanned on an ImageQuant LAS 500 (GE Healthcare Life Sciences).

Immunofluorescence

Transfected HEK293 cells were fixed for 40 min in PBS—2% paraformaldehyde, washed 3 times in ice—cold PBS, permeabilized in PBS—0.1% Triton for 20 min, and then blocked in blocking buffer (4% BSA and 0.05% Tween 20) for 60 min at 4°C. Cells were incubated with anti-FLAG M2 antibody (1:750), produced in mouse, overnight at 4°C, followed by Alexa Fluor 488 anti-mouse IgG (H+L) (1:1,000; Thermo Fisher Scientific) for 1 h at room temperature (RT). After counterstaining with 3 μL of Vectashield antifade mounting medium with DAPI (1.5 μg/mL, Vector Laboratories), cells were visualized using confocal microscopy (Zeiss LSM170 Airyscan). Immunofluorescence experiments were performed in triplicate, with 3 independent transfections and 3 independent plasmid preparations. Cellular localization was determined for each cell on at least 4 fields (on average, 50 cells per variant), and the proportions of nuclear versus cytoplasmic localization for each variant were compared to the WT using one-way ANOVA with uncorrected Fisher's least significant difference. A significance threshold (p value) of 0.05 was used.

3D structure predictions and sequence alignments

The structural model for the MED13L protein was obtained from the AlphaFold Protein Structure Database, based on the complete UniProt: Q71F56 protein sequence and its distinct subunits: N terminus, C terminus, IDRs, and the MedPIWI-like (P-element Induced WImpy testis) domain.[26] To model the effects of the p.Cys1131Tyr, p.Gly1899Arg, and p.Thr2162Met variants, the protein structure was modified with ChimeraX using the swapaa command.[27] The 3D impact was evaluated with the Phyre2 tool.[28] Conservation analysis of the selected residues was carried out through multiple sequence alignment using ClustalW with UniProt: Q71F56 (*Homo sapiens*), H2NIS6 (*Pongo abelii*), F7FWX5 (*Macaca mulatta*), Q6JPI3 (*Mus musculus*), and Q9UHV7 (MED13, *Homo sapiens*).[29] The localization of conserved residues in the MED13 paralog was examined using the human CDK8 module structure (PDB: 8TQC).[12] The MED13L Cys1131 residue corresponded to MED13 Cys1093, Gly1899 to Gly1863, and Thr2162 to Thr2126.

Results

Phenotypic presentations associated to clustered MED13L missense variants

Phenotypic data were compared for 7 different missense variants identified in 13 patients: p.Pro866Leu[6] ($n = 1$), p.Pro866Ala ($n = 1$, ClinVar: SUB15371444), p.Pro869Ser[6,8] ($n = 3$), p.Pro869Leu ($n = 1$), p.Cys1131Tyr[7] ($n = 1$), p.Gly1899Arg[15] ($n = 3$), and p.Thr2162Met[6,17] ($n = 3$) (Table S1). All variants were *de novo*. Pathogenic missense variants were classified into two groups based on a combination of clinical severity and location within or outside known mutational hotspots.

Variants in exons 15 and 17 (p.Pro866Leu, p.Pro869Ser, and p.Cys1131Tyr) were grouped together due to their position within a highly conserved region (Asp860–Pro879) and their association with more severe phenotypes. The first group was associated with a severe phenotype characterized by epilepsy or abnormal electroencephalogram (EEG) (4/5), severe motor impairment with an inability to walk independently (6/6), and large palpebral fissures in addition to the known facial characteristics (5/5). The p.Cys1131Tyr variant was also linked to a severe motor phenotype; at the age of 6 years, the affected patient was only able to sit independently.[7]

In contrast, variants in exons 25 and 30 (p.Gly1899Arg and p.Thr2162Met) were associated with typical MED13L syndrome presentations, including moderate global developmental delay and facial features such as upslanting palpebral fissures, hypertelorism, bulbous nasal tip, hypotonia, and an open mouth (Table S1).[6,7] The second group lies outside the exon 15—17 hotspot.

In vitro analysis of transient expression of MED13L variants

Western blot analysis of whole-cell extracts from cells transiently expressing 3xFLAG—MED13L WT and mutants revealed single bands at about 245 kDa (Figure 1A). In comparison to MED13L WT levels, a significant decrease in protein levels was observed across all conditions. The most pronounced reductions were observed for p.Pro866Leu, p.Cys1131Tyr, and p.Gly1899Arg, with ratios of 0.006, 0.008, and 0.02, respectively ($p < 0.001$). The levels for p.Pro869Ser and p.Thr2162Met exhibited fewer substantial reductions, with values of 0.14 and 0.08, respectively ($p < 0.001$) (Figure 1B).

Cellular localization of MED13L mutant proteins

Immunofluorescence assays were conducted in the HEK293 cell line following transfection with various MED13L mutants. The majority of cells exhibited nuclear localization for the WT and the p.Pro869Ser mutant, with nuclear-to-cytoplasmic ratios of 80:20 and 70:30, respectively. In contrast, the other mutant conditions demonstrated a significant alteration in cellular localization, with predominant cytoplasmic translocation observed for p.Pro866Leu, p.Cys1131Tyr, p.Gly1899Arg, and p.Thr2162Met (Figure 1C). The ratios for these conditions were 34:66, 45:55, 30:70, and 25:75, respectively (Figure 1D).

Interaction between MED13L and CKM complex subunit

To evaluate the capacity of WT or mutant MED13L to interact with MED12 and CDK8, co-immunoprecipitation experiments were conducted with equivalent expression levels in the input samples. Utilizing an anti—FLAG antibody for immunoprecipitation, MED12 and CDK8 antibody signals were detected with comparable band intensity for the WT, p.Pro866Leu, p.Pro869Ser, p.Cys1131Tyr, and p.Thr2162Met mutants. The intensity of the anti-MED12 and anti-CDK8 signals was diminished solely in the recurrent p.Gly1899Arg mutant (Figure 1E). The potential reduction in interactions between the p.Gly1899Arg variant and other members of the CKM was further corroborated in a subsequent co—immunoprecipitation experiment targeting MED12, CDK8, and cyclin-C (Figure 1F).

Residue conservation and 3D structural protein models

The pathogenic missense variants were localized within the IDR of the MED13L protein for p.Pro866Leu and p.Pro869Ser, between the IDR and the MedPIWI-like domain for p.Cys1131Tyr, and in the C-terminal domain for p.Gly1899Arg and p.Thr2162Met (Figure 2A). All variants involved highly interspecies conserved residues that are also conserved in the human paralog MED13 protein (Figure 2B). 3D models were generated for 3 of the 5 pathogenic missense variants. As p.Pro866Leu and p.Pro869Ser involve residues located in an IDR domain with very low model confidence scores according to the AlphaFold prediction tool, models for these variants were not provided.[26]

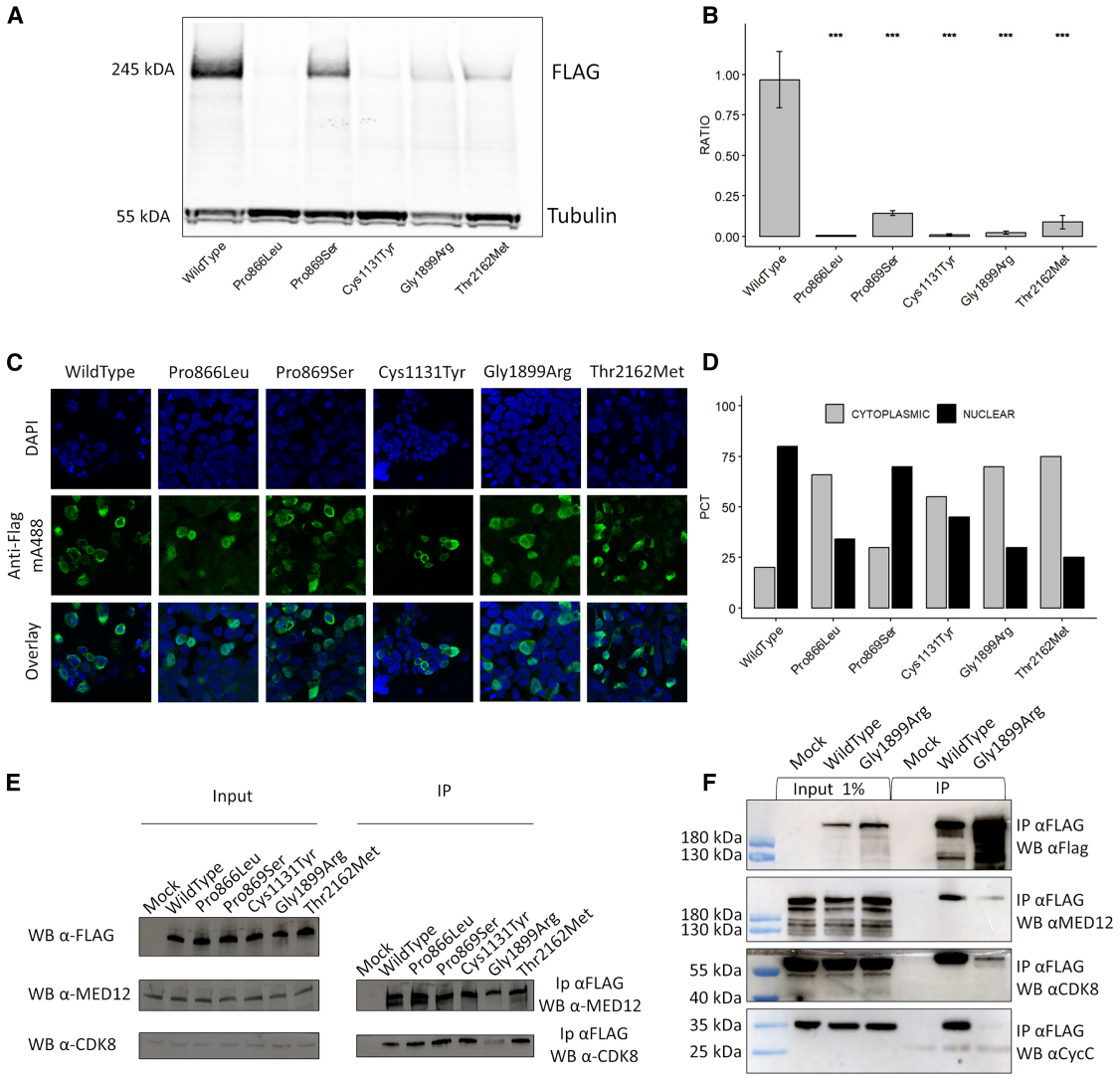

Figure 1. Localization, stability, and integration of pathogenic missense variants

(A) Western blot showing protein levels in cells expressing wild-type or mutant MED13L.

(B) Relative quantification of total MED13L protein levels under different conditions. A significant decrease in MED13L levels was observed in all mutant conditions, with the greatest instability associated with p.Pro866Leu, p.Cys1131Tyr, and p.Gly1899Arg. Statistical comparisons between wild-type and mutant MED13L were performed using a t test (***$p < 0.005$).

(C and D) Immunofluorescence studies revealed a nuclear localization for the wild-type condition, while all protein alterations except p.Pro869Ser showed an altered localization.

(E and F) Co-immunoprecipitation assays showed a reduced interaction between the p.Gly1899Arg variant of MED13L and MED12, CDK8, and cyclin—C. The 3xFLAG blot of input samples confirms equal expression of wild-type and mutant MED13L.

The residue Cys1131 is in the central region of the protein and is in proximity to several residues that participate in hydrogen bonding between the N- and C-terminal regions. These interactions include Arg1126 with Phe169, Arg1126 with Ser1958, Asn1127 with Leu171, Asp1129 with Arg1903, and Ser1130 with both Glu1954 and Lys2129 (Figure 2C). The substitution of Cys1131 with Tyr1131 is predicted to introduce steric clashes with residues Gln2093, Pro2094, and Phe1128. This spatial overlap implies potential structural instability that may disrupt proper protein folding. Furthermore, the substitution is predicted to result in the formation of a novel hydrogen bond with Cys1136, which could modify the rigidity of the protein structure (Figure 2D).[28] The recurrent pathogenic variant p.Gly1899Arg is located within a predicted β sheet secondary structure. This residue forms hydrogen bonds with Tyr1830 and Val1951 (Figure 2E), which are anticipated to be preserved following the substitution of Gly1899 with Arg1899. However, the p.Gly1899Arg substitution replaces a small, buried, and uncharged glycine residue with a bulky, positively charged arginine residue. This change is predicted to introduce steric clashes with nearby residues Val1951, Met1953, and Phe2196, potentially disrupting the local structural integrity (Figure 2F).[28] The recurrent p.Thr2162Met mutant also involves a highly conserved residue near Lys2160, a known

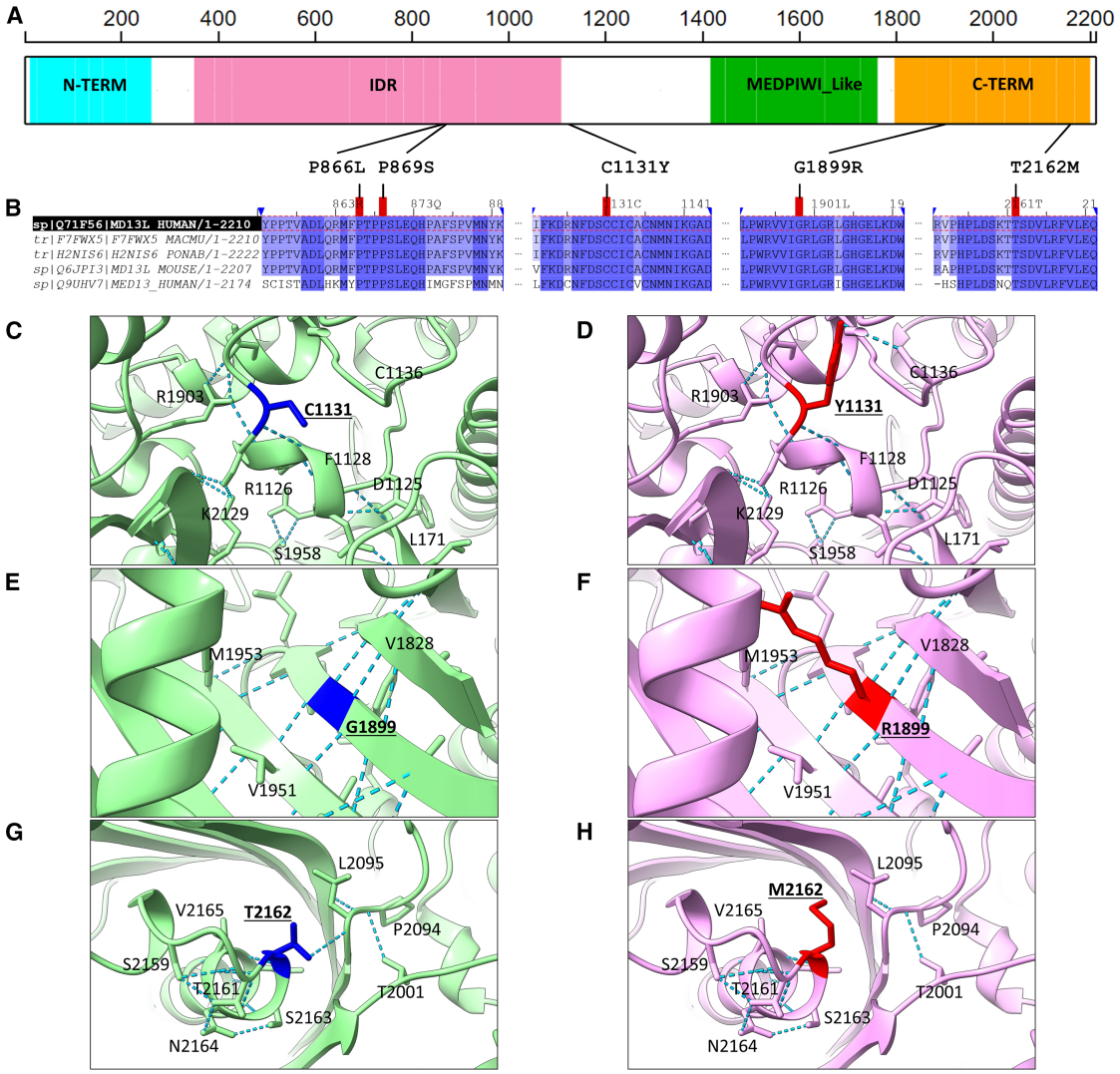

Figure 2. MED13L conservation and structural predictions

(A) Schematic representation of human MED13L highlighting conserved N- and C-terminal domains, a potential intrinsically disordered region (IDR), and the predicted PIWI-like domain.

(B) Multiple sequence alignment showing the conservation of Pro866, Pro869, Cys1131, Gly1899, and Thr2162 residues across species.

(C and D) Wild-type and predicted mutant conformations and interactions for the p.Cys1131Tyr substitution. The predicted hydrogen bond between Cys1131 and Phe1128 stabilizes an α helix formed by residues Arg1126-Asn1127-Phe1128-Asp1129-Ser1130, which participates in interactions with both the N- and C-terminal regions of the protein. Substitution with Tyr1131 is predicted to create a new interaction with residue Cys1136.

(E and F) Wild-type and predicted mutant conformations and interactions for the p.Gly1899Arg substitution. The Gly1899 residue is part of a β strand and contributes to an 8-stranded antiparallel β sheet structure. Substitution of the buried Gly1899 with Arg1899 is predicted to cause a steric clash with surrounding residues within the β sheet structure.

(G and H) Wild-type and predicted mutant conformations and interactions for the p.Thr2162Met substitution. The side chain of Thr2162 forms hydrogen bonds with residues Leu2166 and Leu2095, the latter being lost upon the introduction of Met2162.

Reference and alternative residues are underlined in (C)–(H).

ubiquitination site (Figure 2G). The substitution of Thr2162 is predicted to alter hydrogen bonding by breaking the bond with Leu2095 (Figure 2H).

Discussion

MED13L—related intellectual disability syndrome is characterized by a combination of speech impairment, motor delay, intellectual disability, and distinctive facial features.[1,2,4] In this study, we investigated five pathogenic missense variants identified in patients with the more severe spectrum of the disease, involving residues Pro866, Pro869, and Cys1131. In addition, we included two recurrent missense variants, p.Gly1899Arg and p.Thr2162Met, that were identified in patients with the typical MED13L syndrome phenotype.[15,16,21]

Exon 15 of *MED13L*, which encodes part of the IDR, has been identified as a hotspot for pathogenic variants. Due to the very low confidence score for the predicted

structure of the IDR, modeling of the protein IDR associated with exon 15 was not feasible.[26] However, the domain spanning residues Asp860 to Pro879 appears to be critical for *MED13L* function, as heterozygous missense variants such as c.2579A>G p.Asp860Gly, c.2591T>A p.Met864Lys, c.2590A>T p.Met864Leu, c.2596C>G p.Pro866Ala, c.2597C>T p.Pro866Leu, c.2600C>T p.Thr867Ile, c.2605C>G p.Pro869Ala, c.2605C>T p.Pro869Ser, c.2605C>A p.Pro869Thr, c.2633C>T p.Ser878Phe, and c.2636C>T p.Pro879Leu have been reported as pathogenic.[6,8,30,31] Among these, variants p.Pro866Ala, p.Pro866Leu, p.Pro869Ser, and p.Pro869Leu are associated with more severe phenotypes. Affected individuals commonly present with large palpebral fissures in addition to the known facial characteristics (4/4), epilepsy or abnormal EEG (5/5), inability to walk independently (6/6), and severe feeding difficulties (5/6). Clinical data from the novel patient P6, who carries the p.Pro869Leu variant, further corroborate the specific phenotype linked to variants affecting the Pro869 residue (Table S1). Of note, functional analyses were limited to five missense variants due to our focus on investigating one representative substitution at each of the Pro866 and Pro869 residues, which are part of a mutational hotspot.

The precise biological mechanism underlying the severe phenotype is difficult to ascertain since the p.Pro866Leu and p.Pro869Ser variants exhibit differential behavior. We observed that the p.Pro866Leu mutant variant shared similarities with the other studied variants—p.Cys1131Tyr, p.Gly1899Arg, and p.Thr2162Met—with cytoplasmic localization and protein instability, consistent with a loss-of-function pathogenic mechanism, while p.Pro869Ser exhibited more stable protein expression and partial nuclear localization, closely resembling the WT condition, arguing for the dominant-negative effect of the mutant protein or the possibility of a neomorphic effect with dominant or semi-dominant properties. Further studies, including transcriptomic analyses, will be necessary to clarify its precise functional impact. In addition to the alterations in protein stability and cellular localization, it is possible that other mechanisms are implicated in the pathogenic consequences of the p.Pro866Leu and p.Pro869Ser variants. This is particularly relevant given that both mutant proteins retain their capacity to interact with the other CKM subunits. Residues Pro866 and Pro869 are highly conserved and close to several predicted phosphorylation sites, Thr867, Ser870, and Ser878, and are adjacent to proline residues Pro866, Pro868, Pro869, Pro875, and Pro879.[32,33] The exact role of the phosphorylation sites between residues Asp860 and Pro879 remains undetermined. Both residues are located within an IDR, which is defined by a continuous stretch of disorder-promoting residues. IDRs contribute to the formation of large interfaces that interact with multiple partners. Consequently, these domains have been implicated in critical processes, such as orchestrating protein-protein interactions, including signaling and regulatory pathways.[34] Recent advances using cryoelectronic microscopy and cross-linking mass spectrometry have revealed an important role for the IDR in MED13 in blocking the interaction of the MED26 subunit and the carboxyl-terminal domain of RNA Pol II with the core Mediator complex.[11,12] As the phosphorylation sites are also close to several proline residues, we hypothesize that these pathogenic substitutions could alter the phosphorylation state of this part of the IDR. This could lead to a change in structural organization through local proline *cis*/*trans* isomerization, resulting in secondary structure changes and modification of the local folding organization.[35] Therefore, these substitutions could alter the ability of MED26 to interact with the Mediator complex, with a gain— or loss—of—function effect.[11,12]

The pathogenic missense variation p.Cys1131Tyr was associated with a severe motor phenotype and no epilepsy in the reported patient.[7] The mutant variant was associated with putative protein instability, as indicated by low levels detected by western blotting and a shift in cellular localization to the cytoplasmic compartment (Figures 1A–1C). The substitution did not affect the assembly of the CKM. Residue Cys1131 is predicted to C-cap an α helix composed of residues Arg1126—Asn1127—Phe1128—Asp1129—Ser1130. The side chain of Cys1131 is also predicted to form a hydrogen bond with the carboxylate functional group of Phe1128, stabilizing the α helix. This secondary structure is likely to be critical for the proper folding of the MED13L protein, as residues from the α helix are predicted to form hydrogen bonds linking the N-terminal and C-terminal regions of the protein.[12,26] This substitution could affect the stabilization of the α helix, leading to the pathogenic mechanism through loss of function.

The buried Gly1899 residue is located within a β strand that forms part of an 8-stranded antiparallel β sheet structure. The recurrent p.Gly1899Arg variant showed a significant decrease in *ex vivo* stability, possibly due to proteasome degradation.[9] Substitution of the buried Gly1899 with an Arg1899 is predicted to result in a steric clash with surrounding residues within the β sheet organization. This substitution was observed to affect the interactions of MED13L with other CKM components, CDK8, MED12, and Cyclin-C, most likely reducing the integration of the p.Gly1899Arg mutant protein into the CKM module and leading to a loss-of-function mechanism. This finding is consistent with the involvement of Gly1899 in a β sheet, as such structures have been reported to facilitate protein-protein interactions.[36] Similar effects have been described in MED12-related diseases. In cancer, the p.Leu1224Phe variant has been shown to affect binding to MED13L. In Opitz-Kaveggia (MIM: 305450) and Lujan-Fryns (MIM: 309520) syndromes, the p.Arg961Trp and p.Asn1007Ser variants have been associated with abnormalities in CDK8 recruitment.[37,38]

The p.Thr2162Met pathogenic substitution was also located in a hotspot of pathogenic variants, including c.6485C>A p.Thr2162Lys, c.6488C>T p.Ser2163Leu, and

c.6530C>A p.Ser2177Tyr variations.[6,17,39] The side chain of residue Thr2162 is predicted to form a hydrogen bond with the carboxylate functional group of residue Leu2095, which is located at the N terminus of a β strand involved in an antiparallel β sheet structure. The Leu2095—Thr2162 hydrogen bond connects residues Ser2002, Pro2094, Thr2162, and Ser2163, all of which are associated with pathogenic missense variants. The substitution of Thr2162 with Met2162 is predicted to disrupt the interaction with Leu2095. Consequently, the p.Thr2162Met substitution could disrupt the proper folding of MED13L, thereby compromising potentially critical proximity between these residues required for MED13L function, as Lys2160 is predicted to be a ubiquitination site. The cytoplasmic localization and presumed instability of the pathogenic mutant protein, in the context of the typical phenotype observed in patients (Table S1), suggests a loss-of-function rather than a gain—of—function effect of the substitution.[6,17]

Variants in components of the CKM are linked to overlapping neurodevelopmental syndromes through various functional mechanisms. Pathogenic missense variants have been identified in intellectual developmental disorder related to *CDK8* (MIM: 618748) and developmental and epileptic encephalopathy related to *CDK19* (MIM: 618916). Phosphorylation assays have shown decreased kinase activity for pathogenic missense variants in *CDK8*, leading to loss-of-function effects. In contrast, *CDK19* variants exhibit both decreased and increased kinase activity, resulting in either loss- or gain—of—function effects.[40,41] Pathogenic variants in *CDK19* are associated with a phenotype similar to MED13L syndrome, but variants that decrease kinase activity often cause a more severe presentation, including epilepsy, similar to patients with *MED13L* exon 15 missense variants.[41] Pathogenic missense variants in *MED13* are linked to mild to moderate neurodevelopmental disorders (MIM: 618009). Interestingly, these variants cluster within the phosphodegron motif, which is necessary for binding with the SCF—Fbw7 ubiquitin ligase for degradation. This clustering may prevent protein degradation, leading to increased MED13 protein levels.[9,42] No pathogenic missense variants have been described in the phosphodegron of the MED13L protein. Pathogenic variants in *MED12* cause a range of X—linked intellectual disability disorders, including Opitz—Kaveggia, Lujan—Fryns, Ohdo (MIM: 300895), and Hardikar (MIM: 301068) syndromes. Some clinical features overlap between MED13L syndrome and both Opitz—Kaveggia and Lujan—Fryns syndromes, including moderate intellectual disability, poor speech, and facial hypotonia. These similarities make MED13L syndrome more closely related to MED12 disorders than to MED13 neurodevelopmental syndrome.[15] In addition to variant-specific functional consequences, the clinical variability observed among individuals with MED13L—related disease may be influenced by other factors, including genetic modifiers, epigenetic changes, and environmental influences. Similar multifactorial contributions have been reported in other neurodevelopmental disorders, where background genetic variant and epigenetic regulation modulate the penetrance and severity of phenotypes.[43] Future studies integrating multi-omic approaches may help to identify such modifiers and improve understanding of the variability associated with *MED13L* pathogenic variants.

Functional analysis of MED13L pathogenic missense variations has identified several potential pathogenic mechanisms underlying the disease, highlighting the complexity of functional approaches. These variations are likely to have different effects by affecting one of the many functions of the MED13L protein. This study also suggests potential novel MED13L functions, such as the involvement of exon 15 phosphorylation sites in the MED13L structural conformation, the role of the Gly1899 residue in facilitating interactions that embed MED13L within the CKM, and the critical importance of the MED13L C-terminal domain conformation.

Data and code availability

The datasets used and/or analyzed during the current study available from the corresponding author upon reasonable request.

Acknowledgments

We thank the patients and their families for participating in this study. We thank Delphine Ceraso, Alexis Leurent, Heidi Tampere, and Pauline Grave for their technical assistance with primer design and Sanger experiments, and we thank Samra Holuigue for her technical assistance in cell cultures. This work was generated within the European Reference Network ITHACA. L.A.M. was financially supported by funds of the academic education and research sector plans of the Dutch Ministry of Education, Culture and Science.

Author contributions

T.S. and J.G. wrote the manuscript. T.S., F.F., and M.B. performed the plasmid constructions, western blot experiments, and immunofluorescence studies. T.S., F.F., and C.T. performed the molecular genetic analyses. D.M. and A.V. performed the co-immunoprecipitation assays. R.C., L.A.M., A.N.-S.R., F.P., and J.G. collected and analyzed the clinical and genetic data. T.S., A.V., and J.G. revised the manuscript. All authors participated in the discussion of the results, provided feedback on the manuscript, and approved the final version.

Declaration of interests

The authors declare no competing interests.

Supplemental information

Supplemental information can be found online at https://doi.org/10.1016/j.xhgg.2025.100467.

Web resources

AlphaFold3, https://alphafoldserver.com
ClinVar, https://www.ncbi.nlm.nih.gov/clinvar/
Clustal Omega, https://www.ebi.ac.uk/jdispatcher/msa/clustalo/
GenBank, https://www.ncbi.nlm.nih.gov/genbank/
gnomAD, http://gnomad.broadinstitute.org
OMIM, https://omim.org
PDB, https://www.rcsb.org
UniProt, https://www.uniprot.org
University of California, San Francisco (UCSF) ChimeraX, https://www.cgl.ucsf.edu/chimerax

Received: March 20, 2025
Accepted: June 6, 2025

References

1. Asadollahi, R., Oneda, B., Sheth, F., Azzarello-Burri, S., Baldinger, R., Joset, P., Latal, B., Knirsch, W., Desai, S., Baumer, A., et al. (2013). Dosage changes of MED13L further delineate its role in congenital heart defects and intellectual disability. Eur. J. Hum. Genet. *21*, 1100–1104. https://doi.org/10.1038/ejhg.2013.17.
2. Adegbola, A., Musante, L., Callewaert, B., Maciel, P., Hu, H., Isidor, B., Picker-Minh, S., Le Caignec, C., Delle Chiaie, B., Vanakker, O., et al. (2015). Redefining the MED13L syndrome. Eur. J. Hum. Genet. *23*, 1308–1317. https://doi.org/10.1038/ejhg.2015.26.
3. Cafiero, C., Marangi, G., Orteschi, D., Ali, M., Asaro, A., Ponzi, E., Moncada, A., Ricciardi, S., Murdolo, M., Mancano, G., et al. (2015). Novel de novo heterozygous loss-of-function variants in MED13L and further delineation of the MED13L haploinsufficiency syndrome. Eur. J. Hum. Genet. *23*, 1499–1504. https://doi.org/10.1038/ejhg.2015.19.
4. van Haelst, M.M., Monroe, G.R., Duran, K., van Binsbergen, E., Breur, J.M., Giltay, J.C., and van Haaften, G. (2015). Further confirmation of the MED13L haploinsufficiency syndrome. Eur. J. Hum. Genet. *23*, 135–138. https://doi.org/10.1038/ejhg.2014.69.
5. Asadollahi, R., Zweier, M., Gogoll, L., Schiffmann, R., Sticht, H., Steindl, K., and Rauch, A. (2017). Genotype-phenotype evaluation of MED13L defects in the light of a novel truncating and a recurrent missense mutation. Eur. J. Med. Genet. *60*, 451–464. https://doi.org/10.1016/j.ejmg.2017.06.004.
6. Smol, T., Petit, F., Piton, A., Keren, B., Sanlaville, D., Afenjar, A., Baker, S., Bedoukian, E.C., Bhoj, E.J., Bonneau, D., et al. (2018). MED13L-related intellectual disability: involvement of missense variants and delineation of the phenotype. Neurogenetics *19*, 93–103. https://doi.org/10.1007/s10048-018-0541-0.
7. Tørring, P.M., Larsen, M.J., Brasch-Andersen, C., Krogh, L.N., Kibæk, M., Laulund, L., Illum, N., Dunkhase-Heinl, U., Wiesener, A., Popp, B., et al. (2019). Is MED13L-related intellectual disability a recognizable syndrome? Eur. J. Med. Genet. *62*, 129–136. https://doi.org/10.1016/j.ejmg.2018.06.014.
8. Yi, Z., Zhang, Y., Song, Z., Pan, H., Yang, C., Li, F., Xue, J., and Qu, Z. (2020). Report of a de novo c.2605C > T (p.Pro869Ser) change in the MED13L gene and review of the literature for MED13L-related intellectual disability. Ital. J. Pediatr. *46*, 95. https://doi.org/10.1186/s13052-020-00847-y.
9. Davis, M.A., Larimore, E.A., Fissel, B.M., Swanger, J., Taatjes, D.J., and Clurman, B.E. (2013). The SCF–Fbw7 ubiquitin ligase degrades MED13 and MED13L and regulates CDK8 module association with Mediator. Genes Dev. *27*, 151–156. https://doi.org/10.1101/gad.207720.112.
10. Soutourina, J. (2018). Transcription regulation by the Mediator complex. Nat. Rev. Mol. Cell Biol. *19*, 262–274. https://doi.org/10.1038/nrm.2017.115.
11. Zhao, H., Li, J., Xiang, Y., Malik, S., Vartak, S.V., Veronezi, G. M.B., Young, N., Riney, M., Kalchschmidt, J., Conte, A., et al. (2024). An IDR-dependent mechanism for nuclear receptor control of Mediator interaction with RNA polymerase II. Mol. Cell *84*, 2648–2664.e10. https://doi.org/10.1016/j.molcel.2024.06.006.
12. Chao, T.-C., Chen, S.-F., Kim, H.J., Tang, H.-C., Tseng, H.-C., Xu, A., Palao, L., Khadka, S., Li, T., Huang, M.-F., et al. (2024). Structural basis of the human transcriptional Mediator regulated by its dissociable kinase module. Mol. Cell *84*, 3932–3949.e10. https://doi.org/10.1016/j.molcel.2024.09.001.
13. Daniels, L. (2013). Mutual Exclusivity of MED12/MED12L, MED13/13L, and CDK8/19 Paralogs Revealed within the CDK-Mediator Kinase Module. J. Proteomics Bioinform. *1*. https://doi.org/10.4172/jpb.S2-004.
14. Tsai, K.-L., Sato, S., Tomomori-Sato, C., Conaway, R.C., Conaway, J.W., and Asturias, F.J. (2013). A conserved Mediator-CDK8 kinase module association regulates Mediator-RNA polymerase II interaction. Nat. Struct. Mol. Biol. *20*, 611–619. https://doi.org/10.1038/nsmb.2549.
15. Caro-Llopis, A., Rosello, M., Orellana, C., Oltra, S., Monfort, S., Mayo, S., and Martinez, F. (2016). De novo mutations in genes of mediator complex causing syndromic intellectual disability: mediatorpathy or transcriptomopathy? Pediatr. Res. *80*, 809–815. https://doi.org/10.1038/pr.2016.162.
16. Deciphering Developmental Disorders Study (2017). Prevalence and architecture of de novo mutations in developmental disorders. Nature *542*, 433–438. https://doi.org/10.1038/nature21062.
17. Bowling, K.M., Thompson, M.L., Amaral, M.D., Finnila, C.R., Hiatt, S.M., Engel, K.L., Cochran, J.N., Brothers, K.B., East, K. M., Gray, D.E., et al. (2017). Genomic diagnosis for children with intellectual disability and/or developmental delay. Genome Med. *9*, 43. https://doi.org/10.1186/s13073-017-0433-1.
18. Kaplanis, J., Samocha, K.E., Wiel, L., Zhang, Z., Arvai, K.J., Eberhardt, R.Y., Gallone, G., Lelieveld, S.H., Martin, H.C., McRae, J.F., et al. (2020). Evidence for 28 genetic disorders discovered by combining healthcare and research data. Nature *586*, 757–762. https://doi.org/10.1038/s41586-020-2832-5.
19. Zhou, X., Feliciano, P., Shu, C., Wang, T., Astrovskaya, I., Hall, J.B., Obiajulu, J.U., Wright, J.R., Murali, S.C., Xu, S.X., et al. (2022). Integrating de novo and inherited variants in 42,607 autism cases identifies mutations in new moderate-risk genes. Nat. Genet. *54*, 1305–1319. https://doi.org/10.1038/s41588-022-01148-2.
20. Timberlake, A.T., McGee, S., Allington, G., Kiziltug, E., Wolfe, E.M., Stiegler, A.L., Boggon, T.J., Sanyoura, M., Morrow, M., Wenger, T.L., et al. (2023). De novo variants implicate chromatin modification, transcriptional regulation, and retinoic acid signaling in syndromic craniosynostosis. Am. J. Hum. Genet. *110*, 846–862. https://doi.org/10.1016/j.ajhg.2023.03.017.

21. Kosmicki, J.A., Samocha, K.E., Howrigan, D.P., Sanders, S.J., Slowikowski, K., Lek, M., Karczewski, K.J., Cutler, D.J., Devlin, B., Roeder, K., et al. (2017). Refining the role of de novo protein-truncating variants in neurodevelopmental disorders by using population reference samples. Nat. Genet. *49*, 504–510. https://doi.org/10.1038/ng.3789.
22. Turner, T.N., Wilfert, A.B., Bakken, T.E., Bernier, R.A., Pepper, M.R., Zhang, Z., Torene, R.I., Retterer, K., and Eichler, E.E. (2019). Sex-Based Analysis of De Novo Variants in Neurodevelopmental Disorders. Am. J. Hum. Genet. *105*, 1274–1285. https://doi.org/10.1016/j.ajhg.2019.11.003.
23. Bessenyei, B., Balogh, I., Mokánszki, A., Ujfalusi, A., Pfundt, R., and Szakszon, K. (2022). MED13L-related intellectual disability due to paternal germinal mosaicism. Cold Spring Harb. Mol. Case Stud. *8*, a006124. https://doi.org/10.1101/mcs.a006124.
24. Wilson, K., Newbury, D.F., and Kini, U. (2023). Analysis of exome data in a UK cohort of 603 patients with syndromic orofacial clefting identifies causal molecular pathways. Hum. Mol. Genet. *32*, 1932–1942. https://doi.org/10.1093/hmg/ddad023.
25. Hamada, N., Iwamoto, I., and Nagata, K.-I. (2023). MED13L and its disease-associated variants influence the dendritic development of cerebral cortical neurons in the mammalian brain. J. Neurochem. *165*, 334–347. https://doi.org/10.1111/jnc.15783.
26. Jumper, J., Evans, R., Pritzel, A., Green, T., Figurnov, M., Ronneberger, O., Tunyasuvunakool, K., Bates, R., Žídek, A., Potapenko, A., et al. (2021). Highly accurate protein structure prediction with AlphaFold. Nature *596*, 583–589. https://doi.org/10.1038/s41586-021-03819-2.
27. Meng, E.C., Goddard, T.D., Pettersen, E.F., Couch, G.S., Pearson, Z.J., Morris, J.H., and Ferrin, T.E. (2023). UCSF ChimeraX: Tools for structure building and analysis. Protein Sci. *32*, e4792. https://doi.org/10.1002/pro.4792.
28. Ittisoponpisan, S., Islam, S.A., Khanna, T., Alhuzimi, E., David, A., and Sternberg, M.J.E. (2019). Can Predicted Protein 3D Structures Provide Reliable Insights into whether Missense Variants Are Disease Associated? J. Mol. Biol. *431*, 2197–2212. https://doi.org/10.1016/j.jmb.2019.04.009.
29. Sievers, F., and Higgins, D.G. (2014). Clustal omega. Curr. Protoc. Bioinform. *48*, 3.13.1–3.13.16. https://doi.org/10.1002/0471250953.bi0313s48.
30. Gilissen, C., Hehir-Kwa, J.Y., Thung, D.T., van de Vorst, M., van Bon, B.W.M., Willemsen, M.H., Kwint, M., Janssen, I.M., Hoischen, A., Schenck, A., et al. (2014). Genome sequencing identifies major causes of severe intellectual disability. Nature *511*, 344–347. https://doi.org/10.1038/nature13394.
31. Thiffault, I., Farrow, E., Zellmer, L., Berrios, C., Miller, N., Gibson, M., Caylor, R., Jenkins, J., Faller, D., Soden, S., and Saunders, C. (2019). Clinical genome sequencing in an unbiased pediatric cohort. Genet. Med. *21*, 303–310. https://doi.org/10.1038/s41436-018-0075-8.
32. Hornbeck, P.V., Zhang, B., Murray, B., Kornhauser, J.M., Latham, V., and Skrzypek, E. (2015). PhosphoSitePlus, 2014: mutations, PTMs and recalibrations. Nucleic Acids Res. *43*, D512–D520. https://doi.org/10.1093/nar/gku1267.
33. Wang, D., Liu, D., Yuchi, J., He, F., Jiang, Y., Cai, S., Li, J., and Xu, D. (2020). MusiteDeep: a deep-learning based webserver for protein post-translational modification site prediction and visualization. Nucleic Acids Res. *48*, W140–W146. https://doi.org/10.1093/nar/gkaa275.
34. Fuxreiter, M., Tóth-Petróczy, Á., Kraut, D.A., Matouschek, A., Lim, R.Y.H., Xue, B., Kurgan, L., Uversky, V.N., and Uversky, V.N. (2014). Disordered proteinaceous machines. Chem. Rev. *114*, 6806–6843. https://doi.org/10.1021/cr4007329.
35. Newcombe, E.A., Delaforge, E., Hartmann-Petersen, R., Skriver, K., and Kragelund, B.B. (2022). How phosphorylation impacts intrinsically disordered proteins and their function. Essays Biochem. *66*, 901–913. https://doi.org/10.1042/EBC20220060.
36. Remaut, H., and Waksman, G. (2006). Protein-protein interaction through beta-strand addition. Trends Biochem. Sci. *31*, 436–444. https://doi.org/10.1016/j.tibs.2006.06.007.
37. Kämpjärvi, K., Kim, N.H., Keskitalo, S., Clark, A.D., von Nandelstadh, P., Turunen, M., Heikkinen, T., Park, M.J., Mäkinen, N., Kivinummi, K., et al. (2016). Somatic MED12 mutations in prostate cancer and uterine leiomyomas promote tumorigenesis through distinct mechanisms. Prostate *76*, 22–31. https://doi.org/10.1002/pros.23092.
38. Zhou, H., Spaeth, J.M., Kim, N.H., Xu, X., Friez, M.J., Schwartz, C.E., and Boyer, T.G. (2012). MED12 mutations link intellectual disability syndromes with dysregulated GLI3-dependent Sonic Hedgehog signaling. Proc. Natl. Acad. Sci. USA *109*, 19763–19768. https://doi.org/10.1073/pnas.1121120109.
39. Aoi, H., Mizuguchi, T., Ceroni, J.R., Kim, V.E.H., Furquim, I., Honjo, R.S., Iwaki, T., Suzuki, T., Sekiguchi, F., Uchiyama, Y., et al. (2019). Comprehensive genetic analysis of 57 families with clinically suspected Cornelia de Lange syndrome. J. Hum. Genet. *64*, 967–978. https://doi.org/10.1038/s10038-019-0643-z.
40. Uehara, T., Abe, K., Oginuma, M., Ishitani, S., Yoshihashi, H., Okamoto, N., Takenouchi, T., Kosaki, K., and Ishitani, T. (2020). Pathogenesis of CDK8-associated disorder: two patients with novel CDK8 variants and in vitro and in vivo functional analyses of the variants. Sci. Rep. *10*, 17575. https://doi.org/10.1038/s41598-020-74642-4.
41. Zarate, Y.A., Uehara, T., Abe, K., Oginuma, M., Harako, S., Ishitani, S., Lehesjoki, A.-E., Bierhals, T., Kloth, K., Ehmke, N., et al. (2021). CDK19-related disorder results from both loss-of-function and gain-of-function de novo missense variants. Genet. Med. *23*, 1050–1057. https://doi.org/10.1038/s41436-020-01091-9.
42. Snijders Blok, L., Hiatt, S.M., Bowling, K.M., Prokop, J.W., Engel, K.L., Cochran, J.N., Bebin, E.M., Bijlsma, E.K., Ruivenkamp, C.A.L., Terhal, P., et al. (2018). De novo mutations in MED13, a component of the Mediator complex, are associated with a novel neurodevelopmental disorder. Hum. Genet. *137*, 375–388. https://doi.org/10.1007/s00439-018-1887-y.
43. Parenti, I., Rabaneda, L.G., Schoen, H., and Novarino, G. (2020). Neurodevelopmental Disorders: From Genetics to Functional Pathways. Trends Neurosci. *43*, 608–621. https://doi.org/10.1016/j.tins.2020.05.004.

HGGA, Volume *6*

Supplemental information

MED13L pathogenic missense variants impair protein stability and interaction, underlying diverse clinical outcomes

Thomas Smol, Frédéric Frenois, Morgane Billotte, Roseline Caumes, Leonie A. Menke, Amara Nassar-Sheikh Rashid, Caroline Thuillier, Didier Monté, Florence Petit, Alexis Verger, and Jamal Ghoumid

Supplementary Note: Case Report – patient 6

A 3.24-year-old child harboring a *de novo* heterozygous missense variant in *MED13L* (c.2606C>T; p.Pro869Leu) presented with severe developmental delay, profound speech impairment limited to vocalizations, and global motor delay. Growth parameters were significantly impaired, with a height of 88.0 cm (−2.84 SDS), weight of 8.6 kg (weight-for-height −5.6 SDS), and head circumference of 45.5 cm (−2.5 SDS). Neurological examination revealed hypotonia, while hypertonia and ataxia were absent.

Brain MRI identified a slightly shortened corpus callosum, steep Sylvian fissures, and bilateral incomplete hippocampal folding. EEG was abnormal, with irregular background activity and focal frontal abnormalities, though no epileptiform discharges or clinical seizures were confirmed. Behavioral concerns included significant sleep disturbances, but autism spectrum features were not assessed.

Craniofacial features included a sloping forehead, bulbous nasal bridge and tip, Cupid-bow upper lip, thin vermillion border, hypotonic open-mouth appearance, small, low-set ears, but without significant facial asymmetry or common dysmorphisms such as epicanthus or hypertelorism. The patient had no congenital heart defects, with normal ECG and echocardiography.

Feeding difficulties were profound, requiring tube feeding, and were complicated by cyclic vomiting necessitating a Roux-en-Y jejunostomy, with persistent failure to thrive despite medical therapy. Additional history revealed that the patient has a motility disorder of the gut, contributing to the cyclic vomiting. Although duodenal feeding has been implemented, the patient continues to experience weekly episodes of vomiting, which only resolve when feeding is temporarily replaced with oral rehydration solution (ORS), further complicating nutritional status and weight gain.

Additional anomalies included unilateral hypoplastic cochlear nerve, bilateral severe visual impairment, hemisacralisation of L5, and scoliosis up to 35 degrees.

Supplementary Table S1: phenotypic description of patients carrying pathogenic *MED13L* missense variants

Patient	1	2	3	4	5	6	7	8	9	10	11
Reference	Smol *et al.* (P20)	DECIPHER #268019	Smol *et al.* (P28)	Smol et al (P35)	Yi *et al.*	Present study	Torring *et al.*	Caro-Llopis *et al.*	Bessenyei *et al.*	Smol *et al.* (P14)	Bowling *et al.*
MED13L variants	p.Pro866Leu	p.Pro866Ala	p.Pro869Ser	p.Pro869Ser	p.Pro869Ser	p.Pro869Leu	p.Cys1131Tyr	p.Gly1899Arg	p.Gly1899Arg	p.Thr2162Met	p.Thr2162Met
Inheritance patterns	*de novo*	*de novo*	*de novo*	*de novo*	*de novo*	*de novo*	*de novo*	*de novo*	*de novo*	*de novo*	*de novo*
Age at examination	15 y.	NA	12 y.	24 y.	4y.5m.	3y. 3m.	6 y.	8y	NA	4y.4m.	NA
DD/ID	Severe	Severe	Severe	Severe	Severe	Severe	Severe	Severe	Moderate	Moderate	Moderate
Speech delay	Absent speech	NA	Absent speech	Absent speech	Absent speech	Absent speech	Absent	Absent	Little expressive speech	First words at 4y.	Speech delay
Motor skills	Ability to walk lost at 10y.	NA	No independent walking	Ability to walk lost at 10y.	Severe motor delay No independent walking	Walking not acquired	Head control, no independent sitting	Head control: 7 m., sitting: 17 m.	Delay	Walking at 26m.	NA
Seizure	Late onset infantile spasms	Abnormal EEG and seizure	Yes	Lennox-Gastaut syndrome	No seizure Abnormal EEG (spike and slow wave rapid rhythm)	Abnormal EEG	No seizure	No epilepsy	Focal bilateral abnormal waves on EEG	No seizure	NA
Atypical Neurological findings	ASD	Primary microcephaly	ASD Microcrephaly	No	ASD Microcephaly		Major hypotonia spastic paraparesis, dystonia (extremities and tongue)	ASD with aggressive behavior	No	NA	Microcephaly
Brain MRI	Normal	Agenesis of corpus callosum	Hypoplasia corpus callosum Delayed myelinisation	Diffuse cortical atrophy	Enlarged bilateral lateral ventricles	Slighlty too short corpus callosum; too steep course of Sylvius and incomplete folding of the hippocampus on borh sides	Enlarged ventricular Partial agenesis of the corpus callosum, Dandy-Walker variant	Enlarged peri-cerebral space	Normal	Normal	Normal
Feeding difficulties	Severe weight loss in spite of enteral nutrition	Gastrostomy tube feeding in infancy	Sond-feeded until 3 m. age	Severe weight loss in spite of enteral nutrition	no	Severe weight loss in spite of enteral nutrition – Cyclic vomiting	No	No	No	No	No
Atypical facial feature	Large palpebral fissures	NA	Large palpebral fissures	Large palpebral fissures	NA	Large palpebral fissures	Blepharophimosis	No	Long face	NA	No
Miscellaneous	Nystagmus Craniosynostosis	Retinal dystrophy, severely reduced visual acuity, scoliosis	No	Severe myopia	Odontoprisis, appendicular muscular atrophy, hyperlaxity of the joints, scoliosis, spontaneous facture of femur	Severe visual impairment - Scoliosis	Microphthalmia Bilateral corneal opacities	Renal cyst	No	No	No

ASD: Autism Spectrum Disorder; EEG: Electroencephalography;NA: non-available